



The Application of Artificial Neural Networks to Weld-Induced Deformation in Ship Plate

Data from the weld trials used in the development of the model revealed carbon content plays a key role in distortion

M. P. LIGHTFOOT, G. J. BRUCE, N. A. McPHERSON, AND K. WOODS

ABSTRACT. An artificial neural network model was developed to be used in a study of factors affecting the distortion of 6- to 8-mm-thick D and DH 36 grade steel plate. The data from a significant number of closely controlled welding trials, and subsequent measurements of distortion were input into the model. From this model development, a sensitivity analysis was carried out, which highlighted a number of apparently key factors, which influenced distortion. From this it was established that the carbon content of the steel plate played a key role in the amount of distortion produced by the welding process. The mechanism of the effect of carbon appears to be linked to its effect on grain size, transformation temperature, mechanical properties and pearlite content at least. It was established that an increase in carbon content was beneficial in reducing thin plate distortion caused by welding.

Introduction

For many years, deformation induced by welding in shipyards has been a common cause of rectification costs. However, this effect is being exacerbated by superstructure and deck plate thickness reductions (Ref. 1), as plate thickness decreases, the extent of deformation tends to increase (Ref. 2). In many cases, the distortion is actually buckling (Ref. 3). A great number of studies have been carried out with various potential solutions to the problem of distortion, but the problem still persists (Refs. 2, 4). There have been

areas of improvement but not elimination. These areas have centered on the quality of the steel plate being used, by improving mill rolling characteristics, and introducing or upgrading cold leveling facilities (Ref. 5). Plate cutting processes have been improved too, with the introduction of techniques such as underwater plasma arc cutting and laser beam cutting (Ref. 6). It has been claimed that both processes minimize the residual stress levels of the cut face, and the depth of the hardened zone. Welding techniques have advanced too, with gradual reductions in heat input being made. The introduction of laser beam welding (Ref. 7) and derivatives of it (Ref. 8), have resulted in quantum steps in heat input reduction being achieved. Consequently, distortion will decrease accordingly.

In parallel with the practical methods of distortion reduction, there have been a number of other approaches. One has been the Risk Shared Management approach (Ref. 9), which has shown some specific benefits. Some preliminary work has been carried out on the application of artificial neural networks to weld distortion (Ref. 10). A number of weld distortion models have been developed (Refs. 11, 12), but suffer from the drawback of predicting symmetrical distortion.

Neural networks find their origin in biological science. However, the basis of

that has been extended to artificial neural networks, which is the general terminology used to describe the mathematical models. A number of studies have shown the benefits of this approach within the welding processes. These are metal transfer (Ref. 13), mechanical properties (Ref. 14), acoustic emission (Ref. 15), and preliminary distortion prediction (Ref. 16). In addition, a review (Ref. 17) of the use of neural networks in materials science was carried out and it refers to a number of areas in the welding process, but not welding distortion.

The basis of a neural network is shown in Fig. 1. This is composed of the following components:

- An input layer that receives signal from the environment
- An output layer that conveys the signals to the environment
- One or more hidden layers that keep some input and output signals within the network itself.

The behavior of the output depends on the activity of the hidden units and the weight assigned between the hidden and output units.

Mathematically, the output can be represented as shown below

$$O = \sum_{n=1}^n I_n * W_n$$

where O = output, I = input, W = weight. These values are vectors and the sum must be calculated for each layer of the neural network.

Experimental

The materials that were used are shown in Table 1. These two steels are typical of those now being adopted in warship construction, with the DH 36 being utilized in areas requiring higher strength (>360 N/mm²), and the D being used in

M. P. LIGHTFOOT and G. J. BRUCE are with the Department of Marine Technology, University of Newcastle, Newcastle upon Tyne, Scotland. N. A. McPHERSON is with BAE Systems, Naval Ships, Glasgow, Scotland. K. WOODS is with Corus Construction and Industrial, South Teesside Works, Redcar, Scotland.

KEY WORDS

Neural Networks
Deformation
Distortion
Ship Construction
Thin Plate

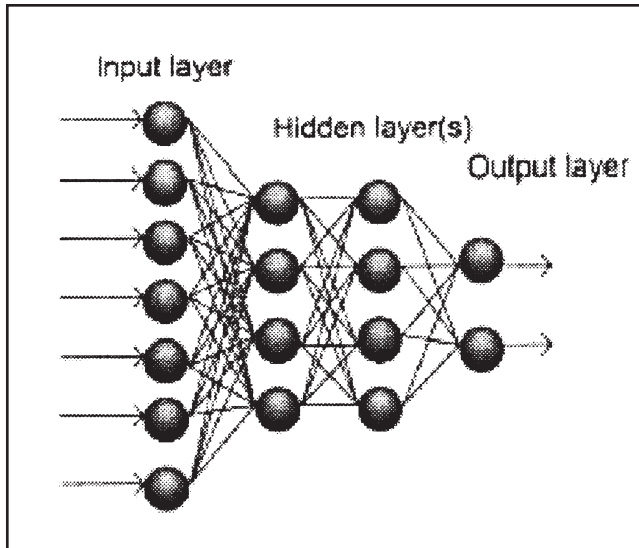


Fig. 1 — Basic concept of a neural network.

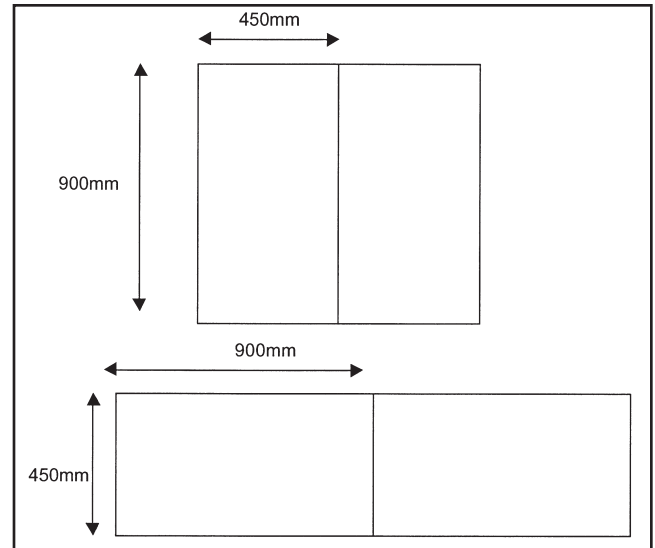


Fig. 2 — Trial plate configurations used in the evaluation.

areas where a minimum strength of 235 N/mm² is acceptable. All the baseplates (5 × 2 m) had been cold leveled, and delivery and storage conditions were similar. Each base plate was shot blasted and paint primed on the same processing line, under ostensibly the same conditions. Table 2 shows the variables that were designed into this study from the supplied plate material. The complete list of variables has been included in Appendix 1.

Table 1 — Main Variables Used in the Evaluation

Plate materials	D Grade	DH 36 Grade
Plate thickness	6 mm 8 mm	6 mm 8 mm
Cutting process	Underwater plasma Laser	Underwater plasma Laser
Variables	4	4

The plate configurations used are shown in Fig. 2, along with dimensions. These configurations were chosen as being relatively common setups within a shipyard. After cutting from the base plate, each plate was marked out with a predetermined square grid to facilitate identification of measurement points (36 for each plate, i.e., 72 for each welded panel). The plates were laid on top of a 25-mm-thick plate that had been milled flat. This was used as the datum for all measurements. The actual measurement was carried out using a movable bridge and a digital depth gauge. Each set of plates was tack welded from the bottom. Measurements were taken after tack welding, and again after welding was completed. In all cases, only DH 36 grade was welded to DH 36 grade, and only D grade was welded to D grade. In addition, only like plate thickness were welded together, always in the rolling direction.

In some instances plates were restrained by welding areas of the longitudi-

nal edge to the base plate on which the welding was being carried out.

Welding was carried out using the flux cored welding process (1.2-mm-diameter wire) with a shielding gas of 80% Ar/20% CO₂. The actual welding utilized a mechanized welding head on a track, to create as much consistency in the welding process as possible. All welding was carried out in the flat position, and the weld preparation was a 60-deg included angle, with a closed root. The angle on the plate edge was produced using a cold mechanical process. Plates were tack welded together from the bottom to a constant procedure. The 6-mm-thick plates were welded with one pass, and the 8-mm-thick plates required two passes, with the inter-pass temperature being less than 100°C in all cases. The range in heat inputs used is given in Appendix 1. No postweld heat treatment was carried out on any of the welded plates.

Distortion measurements were col-
lated on a spreadsheet, and initially the

Table 2 — Chemical Composition (wt-%) and Mechanical Properties of the Base Plate Involved

		%C	%Si	%Mn	%P	%S	%Al	%Nb	%N ₂	CE ^(a)	YS	UTS
DH 36 grade	8 mm thick	0.11	0.27	1.26	0.023	0.008	0.032	0.032	0.004	0.33	493	566
		0.15	0.01 ^(b)	1.36	0.016	0.008	0.029	0.026	0.004	0.38	394	493
	6 mm thick	0.14	0.39	1.4	0.014	0.009	0.033	0.027	0.005	0.38	395	534
		0.14	0.40	1.5	0.015	0.011	0.036	0.027	0.005	0.39	523	607
DH 36 spec		0.18	0.50	0.90	0.030	0.025	0.015	0.02			355	490
		(max)	(max)	1.60	(max)	(max)	(min)	0.05			(min)	620
D grade	8 mm thick	0.10	0.23	0.84	0.017	0.008	0.027	0.001	0.005	0.24	302	422
		0.10	0.23	0.84	0.017	0.008	0.027	0.001	0.005	0.24	432	511 ^(c)
	6 mm thick	0.09	0.27	1.02	0.019	0.007	0.023	0.001	0.009	0.26	333	433
D spec		0.21	0.35	0.6	0.040	0.040	0.015			0.40	235	400
		(max)	(max)	(min)	(max)	(max)	(min)			(max)	(min)	490

(a) CE = C + Mn/6 + (Ni + Cu)/5 + (Cr + Mo + V)/15

(b) Specification relaxation for steels for laser cutting.

(c) Concession on this property

(YS and TS are in N/mm²)

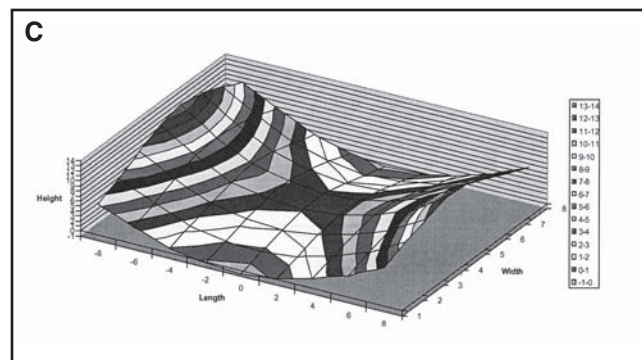
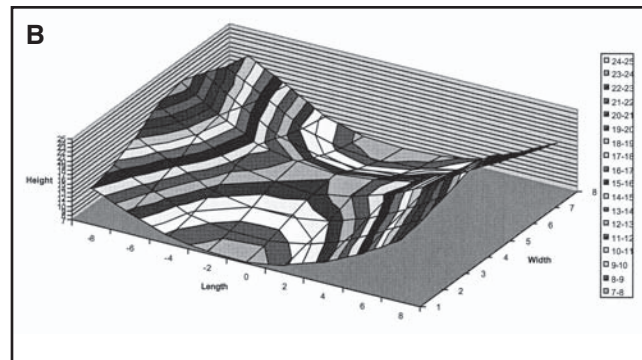
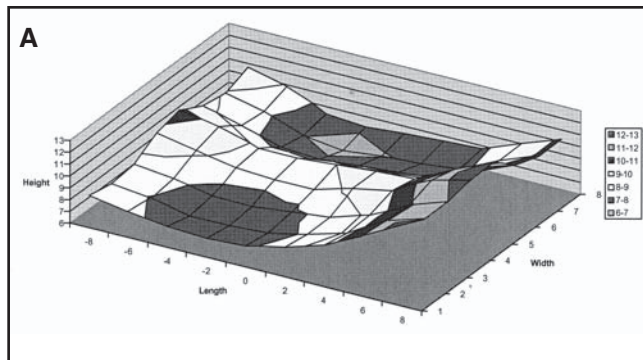


Fig. 3 — A — Test plate profile after welding (height in mm); B — test plate with distortion induced after welding (height in mm); C — actual distortion induced by welding (height in mm).

distortion was categorized using a single figure of the standard deviation of all the measurements on the plate. This was then refined to use I numbers. A description of the I number and the process to use I numbers is contained in Appendix 2. This gave longitudinal and transverse measurements of distortion.

Model Development

In total, 132 test plates were produced, which resulted in 66 small panels being welded up. All data were recorded on Excel spreadsheets, and this allowed graphical representations to be made of surface contours after tack welding, after welding, and of actual distortion. An example of each is shown in Fig. 3A–C.

The main function of this work was to produce enough actual data to initially train an artificial neural network model, and then with the remnant data, test the model.

The following neural network models were considered for selection:

- Multilayer Perceptron (MLP) (Refs. 18–20)
- Generalized Feed-Forward (GFF) (Refs. 18–20)
- Modular Feed-Forward (MFF) (Refs. 18–20)

Multilayer Perceptrons are layered feedforward networks typically trained with back propagation. These networks have found their way into countless applications requiring static pattern classification. Their main advantage is that they are simple to use, and that they can approximate any input/output map. The key disadvantage is that they train slowly and require significant amounts of training data.

The GFFs are a generalization of the MLP, such that connections can jump over one or more layers. In theory, a MLP can solve any problem that a GFF can solve. In practice, generalized feedforward networks often solve the problem much more efficiently.

The MFFs are a special class of MLP. These networks process their input using several parallel PLPs, and then recombine the results. This tends to create some

structure within the topology, which will foster specialization of function in each submodule.

In contrast to the MLP, modular networks do not have full interconnectability between the layers. As a result of this, a smaller number of weights is required for the same size of network. This tends to speed up training times and reduce the number of required training exemplars.

Twenty-eight sets of data for 6-mm-thick plate were used to train the models and three sets were used to test them. The three sets selected for testing were chosen at random from the dataset. The ratio of testing to training was changed but when the model was trained on less data, the accuracy of prediction decreased. By using the basic model topology provided by the software, *NeuroSolutions*, the networks were changed without altering the model topology to find which can cope best with the data set provided. It was found that the MLP model was superior to either the GFF or the MFF. The next step in the model development was to select the number of iterations required to train the network, and when to stop the simulations. The network was trained between 4000 and 16,000 iterations. It was found in this instance that the least number of errors, and therefore the best prediction, was obtained using 16,000 iterations. Following this, the effect of the number of hidden layers on the neural network output had to be determined. The number of hidden layers tested was 1, 3, and 5. It was found that three hidden layers represented the actual surface topology of the weld most accurately. Lastly, a momentum coefficient had to be determined. This is related to the need to speed up the back propagation algorithm without producing oscillations. So, a momentum term is included at each

iteration to incorporate past weight changes and current weight change. The momentum coefficient (a) can have a value of between 0 and 1. The coefficient was varied and this led to a momentum coefficient of 0.5 being chosen to produce the least number of errors in the final prediction.

On this basis, the MLP network architecture configuration was defined as
 Network Model – MLP
 Iterations – 16,000
 Hidden Layers – 3
 Momentum Coefficient – 0.5

The complete network topology cannot be disclosed, at present, due to the nature of the funding for this project.

It was established that by using this configuration, the 6-mm-thick plate situation could be accurately represented. Figure 4A–D are taken from 6-mm-thick material data and compare actual distortion against predicted distortion. Using standard deviation as the measure of actual and predicted distortion, it was found in the case of Fig. 4A and B that the difference between the two data sets was 13% overestimated by the prediction. In the case of Fig. 4C and D, the difference was 18% underestimated from the prediction. In real measurement, these percentage errors are about 2 mm. However, in both situations the direction of distortion was being predicted correctly. This compari-

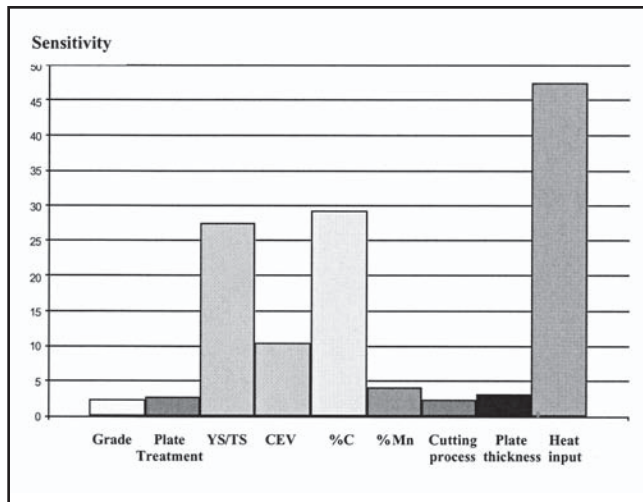


Fig. 5 — Sensitivity analysis of identified key factors related to distortion from the current study.

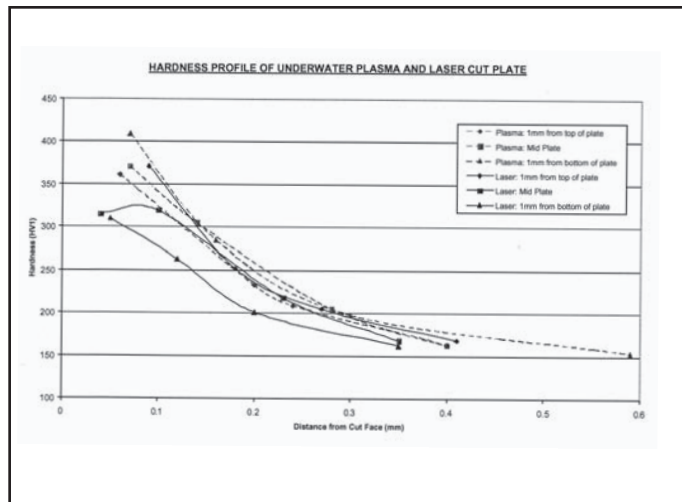


Fig. 6 — Hardness scans of cut edge profile of laser beam cut and underwater plasma arc cut D grade 6-mm-thick plate.

distortion, and to some extent help validate the accuracy of the model outputs. Two of these factors were that higher heat input produced more distortion, and thinner plate gave more welding-induced distortion. However, other factors that have not been readily identified in the past with distortion, such as CE, yield/tensile strength ratio, steel grade, and plate treatment will now be considered in more detail, from a metallurgical standpoint.

Steel Grade

There was less distortion associated with the DH 36 grade than the D grade, i.e., the higher-strength steel was less distortion sensitive. This could be related to microstructural differences, with there being a tendency to produce a finer grain size in the higher-strength DH 36, due to the presence of niobium in the steel (Ref. 25). In addition, the DH 36 steel had a higher average carbon content than the D grade steel and therefore would have a higher pearlite content, which would reduce the ductility of the plate, making it less susceptible to distortion. A typical figure would be 8 μm for DH 36. However, there is considerable overlap in the range of grain sizes produced for D and DH 36 due to plate thickness effects and other processing factors.

Cutting Process

One relatively surprising result was that the underwater plasma arc cut plates resulted in less distortion after welding. Previous work (Ref. 6) had shown the opposite effect. The plate edge weld preparation in this work was a 30-deg angle. By introducing this, the bulk of the cut face

would be removed. Additional work was carried out using the same 6-mm-thick D grade steel plate, on which a laser beam cut edge and an underwater plasma arc cut edge had been made. This allowed a direct comparison to be made to establish heat-affected zone (HAZ) characteristics, in the actual cut face. These data are shown in Table 4, and the laser beam cut HAZ is slightly narrower on average than the underwater plasma arc cut HAZ. However, there was evidence of a white band in the laser beam cut HAZ and this has in the past been associated with the presence of martensite and by implication higher hardness. Hardness determinations were carried out on the two HAZs and are shown in Fig. 6. It is clear that the underwater plasma arc cut material had the highest overall hardness in the vicinity of the cut face. However, at the bottom of the weld, which would be the only cut face left, the underwater plasma arc cut material was approximately 100 HV1 higher than the laser beam cut material. This difference tapered off on moving back into the base plate. There was no evidence to indicate that the white band had higher hardness than the rest of the area being tested. It also shows that the base plate hardness was reached in all areas approximately 0.3 mm back from the cut face.

At this stage, no firm conclusion can be

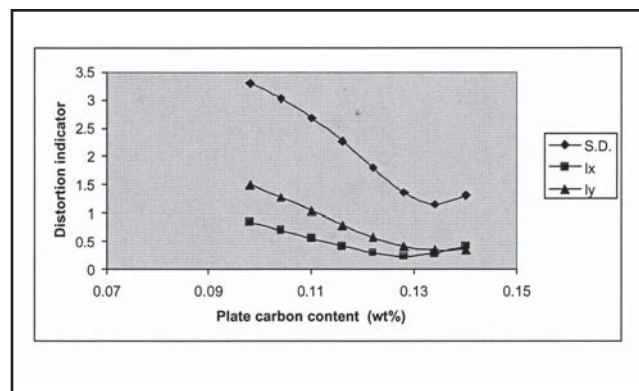


Fig. 7 — Relationship between plate carbon content and distortion after welding: SD = standard deviation; I_x and I_y = I-numbers.

drawn, apart from there being more significant effects than the effect of the cutting process on distortion. Figure 5 does show that the sensitivity of the cutting process is relatively low compared to some of the other factors. However, this does illustrate the need to question the data, and not accept the outcomes at face value.

Carbon Equivalent

The initial view was that as carbon equivalent increased then the distortion decreased. However, in the current steels the main, and most significant, components of carbon equivalent are carbon and manganese (Ref. 25), as shown in Equation 1

$$CE = C + \frac{Mn}{6} + \frac{(Ni + Cu)}{5} + \frac{(Cr + Mo + V)}{15} \quad (1)$$

The sensitivity of carbon and man-

Table 4 — Cut Face Examination Data Summary

Process	Underwater Plasma		Laser	
	HAZ Width (mm)	White Band Present (microns)	HAZ Width (mm)	White Band Present (microns)
Top	0.28	No	0.37	4 to 7
Middle	0.29	No	0.3	3 to 6
Bottom	0.34	No	0.19	No
	Transformation zone (mm)		Transformation zone (mm)	
Top	0.12		0.12	
Middle	0.12		0.1	
Bottom	0.14		0.09	

ganese was tested, and it was quite clear that carbon had the more significant effect. On extracting the data, there was a gradual and consistent reduction in distortion as the carbon content increased. This is shown in Fig. 7, where the standard deviation (SD) and the I-numbers (I_x and I_y) are plotted against the plate carbon content.

Figure 5 clearly shows that the dominant effect within CE is carbon, and there is little effect from manganese. It is well known (Ref. 26) that as the carbon content of the steel increases then the percentage of pearlite present within the microstructure also increases. As a result of this the ductility of the steel decreases making it potentially less liable to distort. In addition to that consideration, Withers and Bhadeshia (Ref. 27) presented data that showed that as the calculated transformation temperature (Ar_3) of the steel decreased the amount of distortion present after welding decreased. Increasing the carbon and manganese content has a similar effect in reducing the transformation start temperature. This would again emphasize the grade effect discussed earlier, with DH 36 having higher carbon and manganese contents.

Yield Strength/Tensile Strength

A starting point for this factor would be the relative relationship between composition and strength. Equations 2 and 3, shown below, are based on work by Pickering and Gladman (Ref. 28).

$$\begin{aligned}
 YS \text{ (N/mm}^2\text{)} &= 53.9 \\
 &+ 32.3\%Mn + 83.2\%Si \\
 &+ 354\%N_f + 17.4d^{-1/2} \quad (2)
 \end{aligned}$$

$$\begin{aligned}
 TS \text{ (N/mm}^2\text{)} &= 294 \\
 &+ 27.7\%Mn + 83.2\%Si \\
 &+ 3.85\%pearlite + 7.7d^{-1/2} \quad (3)
 \end{aligned}$$

where d = ferrite grain diameter in mm and N_f = free nitrogen content.

If the two relationships are considered as being the basis of the YS/TS ratio, the

manganese and silicon components approximately cancel each other out in the ratio. If all the nitrogen is considered to be combined as aluminum nitride, there is no contribution from free nitrogen. However, the increase in carbon content would produce a decrease in grain size due to the lower transformation temperature. This would result in a larger contribution to the positive grain size effect of the yield stress compared to the tensile stress. Using expected grain sizes of $8 \mu\text{m}$, the grain size contribution to yield strength is 192 N/mm^2 , and to tensile strength is 84 N/mm^2 . However, the pearlite content, typically 16%, also has a positive effect on tensile stress. This contributes approximately 65 N/mm^2 . Overall this would lead to a greater YS/TS ratio. It is known (Ref. 25) that the pearlite content of steel increases as the carbon content increases. All other factors being constant, then as the grain size decreases the YS/TS ratio will increase too.

Plate Rolling Treatment

Normalized rolling was the least susceptible process to distortion followed by as-rolled, and then normalized as the most susceptible to distortion. However, there is a significant skew in the relative populations with their being significantly more normalized plates in the study than as-rolled and normalized rolled. It is clear that further work is required in this particular area.

Conclusion

There is clearly significant potential in the application of artificial neural networks to distortion-related issues. However, it is important to recognize that the outputs from the models cannot be taken at face value, and that a scientific understanding to the trends has to be developed too. This has been attempted in the case of the effect of carbon in this specific work. This work has used the sensitivity analysis tool to identify some process aspects that

had a previously unknown contribution to distortion.

A number of distortion-related factors have now been identified that can be specified at the plate stage, such as carbon content, YS/TS ratio, and rolling treatment. The acceptance of these factors will lead to a reduction of cutting- and weld-related distortion in 6 to 8-mm-thick plates, but will certainly not eliminate it.

Acknowledgments

This work was funded by a grant through the Shipbuilders and Shiprepairers Association (SSA), on behalf of the Department of Trade and Industry (DTI). Acknowledgment is gratefully made for the contributions from W. McGhie and J. Gray of BAE Systems, Naval Ships. In addition, the authors most gratefully acknowledge the constructive input from N. I. Cooper of BAE Systems, Submarines, and D. Bucke of the SSA.

References

1. Dydo, J. R., Castner, H. R., and K. Koppenhoefer, K. 1999. Edison Welding Institute, Project No. 42372-GDE.
2. Masubuchi, K. 1980. *Analysis of Welded Structures*, pp. 235–327, Pergamon Press.
3. Michaleris, P., and DeBicari, A. 1996. A predictive technique for buckling analysis of thin section panels due to welding. *Journal of Ship Production* 12(4): 269–275.
4. Radaj, D. 1992. *Heat Effects of Welding*, pp. 1–18, Springer-Verlag.
5. Dunsmore, A. 2003. Private communication, Corus Technology.
6. Russell, J. D., Hilton, P. A., Frost, J. L., and Riches, S. T. 1997. TWI Report No. 8, 8250/1/97.
7. Tsukamoto, S., Kawaguchi, I., Otani, T., Arkane, G., and Honda, H. 2002. Formation mechanism and suppression of welding defects in 20-kW CO_2 laser welding. *Proceedings 6th International Trends in Welding Research Conference*, Pine Mountain, Ga., pp. 459–464.
8. Roland, F. 2002. Laser welding in shipbuilding — an overview of the activities at Meyer Werft. *IIV International Conference, Advanced Processes and Technologies in Welding and Allied Processes*, Copenhagen, Denmark. Paper B-II.
9. Sukovoy, O. 2002. *A Risk Based Methodology for Minimizing Welding Distortion in Steel Ship Production*. Ph.D. thesis, University of Strathclyde.
10. Yuliadi, M. Z. 2000. *A Study on the Topology of Ship Plate Distortion by Neural Networks*, Ph.D. thesis, University of Newcastle, 2000.
11. Porzner, H. 2001. Possibilities of numerical simulation for evaluation and optimization of welded design principles. *Mathematical Modeling of Weld Phenomena 5*. Institute of Materials, pp. 701–723.
12. Doynov, N., Christov, St., Michailov, V.,

and Wohlfahrt, H. 2002. Finite elements simulation of multipass submerged arc welding. *Mathematical Modeling of Weld Phenomena 6*. Maney, pp. 651–669.

13. Stroud, R. R., McArdle, J. R., and Vincent, D. 1994. The application of neural networks to the classification of metal transfer mode in metal inert gas welding. *Proceedings of the 7th International Conference on the Joining of Materials*. Helsingör, Denmark. pp. 459–468.

14. Metzbower, E. A., DeLoach, J. J., Lalam, S. H., and Bhadeshia, H. K. D. H. 2001. Analysis of the strength and ductility of welding alloys for HSLA shipbuilding steels. *Science and Technology of Welding and Joining*, 6(2): 116–124.

15. Taylor Burge, K. L., Harris, T. J., Stroud, R., and McArdle, J. R. 1992. The use of neural networks to characterize problematic arc sounds. *Proceedings of the 4th International Conference on Computer Technology in Welding*. Cambridge, U.K., paper 35.

16. Bruce, G.J., Yuliadai, M. Z., and Shahab, A. 1999. A study on the prediction of ship

plate distortion topology by neural networks. *Journal of Ship Production* 15(4): 191–197.

17. Bhadeshia, H. K. D. H. 1999. Neural networks in materials science. *ISIJ International* 39(10): 966–979.

18. Nelson, M. C., and Illingworth, W. T. 1991. *A Practical Guide to Neural Nets*, Addison-Wesley Publishing.

19. Fausett, L. 1994. *Fundamentals of Neural Networks — Architectures, Algorithms and Application*, Vol. 1, Prentice-Hall Publishing.

20. Haykin, S. 1999. *Neural Networks — A Comprehensive Foundation*, 2nd Edition, Prentice-Hall Publishing.

21. Yang, Y. P., Brust, F. W., Cao, Z., Kennedy, J. C., Chen, X. L., Yang, Z., and Chen, N. 2002. Weld modeling technology for shipbuilding applications. *6th International Trends in Welding Research Conference Proceedings*. Pine Mountain, Ga., pp. 855–860.

22. PREDICTOR. 2003. Distortion prediction software package, University of Newcastle.

23. Camilleri, D. 2004. Private communication, University of Strathclyde.

24. Yang, Y. P., Brust, F. W., Ezeilo, A., and McPherson, N. 2004. Weld modeling of thin structures with VFT software. Presented at 2004 ASME Pressure Vessels and Piping Conference, San Diego, Calif.

25. Llewellyn, D. T. 1994. *Steels — Metallurgy and Applications*. Butterworth Heinemann, 2nd Edition. pp. 118–119.

26. Smallman, R. E., 1970. *Modern Physical Metallurgy*, Butterworth and Co. 3rd Edition. pp. 454–456

27. Withers, P. J., and Bhadeshia, H. K. D. H. 2001. Residual stress part 2 — nature and origins. *Materials Science and Technology*, 17: 366–375

28. Pickering, F. B., and Gladman, T. 1961. An investigation into some of the factors which control the strength of carbon steels. ISI Special Report 81, pp. 10–20. The Iron and Steel Institute.

29. Paakkari, J. 1998. Tech. D. Dissertation, University of Oulu, Finland.

Appendix 1

Model Inputs

Steel grade	D and DH 36
Plate rolling treatment	Normalized: Normalized rolled: As-rolled
Yield strength (N/mm ²)	302–523
Tensile strength (N/mm ²)	422–607
Yield/Tensile strength	0.716–0.871
% elongation	24–39
Plate cutting process	Underwater plasma arc and laser beam
Length (mm)	450 and 900
Width(mm)	900

Length/width	and 1800
Plate thickness (mm)	0.25 and 1.0
Length/thickness	6 and 8
Welding voltage (V)	56–150
Welding current (A)	21–27
Travel speed (mm/min)	225–275
Welding heat input (kJ/mm)	210–360
	1.013–1.616

(raw heat input—not corrected with arc efficiency)

Carbon equivalent (CE)	0.24–0.39
Plate chemistry	
% carbon	0.09–0.15
% silicon	0.01–0.40
% manganese	0.84–1.50
% phosphorus	0.011–0.023
% sulfur	0.007–0.012

% chromium	0.013–0.017
% nickel	0.017–0.020
% molybdenum	0.002–con stant
% aluminum	0.023–0.036
% copper	0.005–0.010
% niobium	0.001–0.032
% nitrogen	0.004–0.009
% tin	0.001– 0.003
% titanium	0.001–0.002
% vanadium	0.002–con stant

Initial surface topology at 72 points after tack welding
Surface topology at 72 points after welding
Induced distortion at 72 points after welding (after welding—after tack welding)

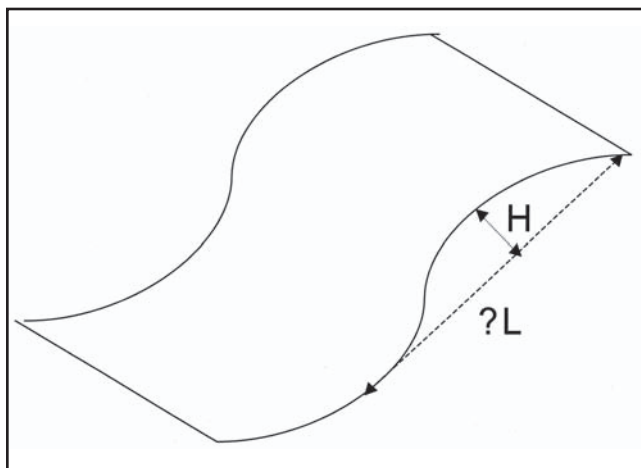


Fig. 8 — Example of sheet metal exhibiting edge waves.

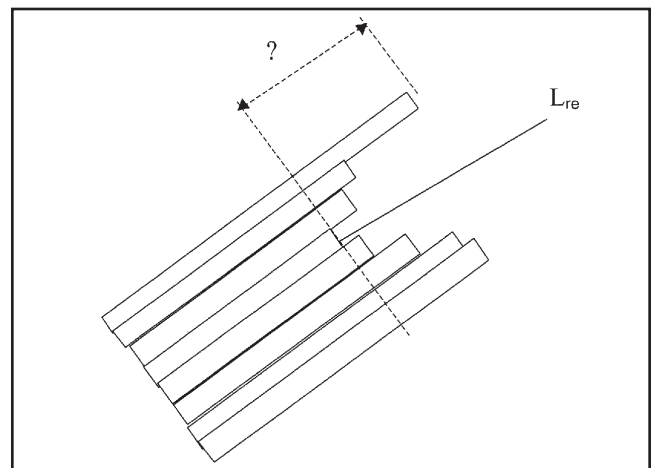


Fig. 9 — Elastic stresses are relaxed when a series of lengthwise cuts is made in the sheet metal.

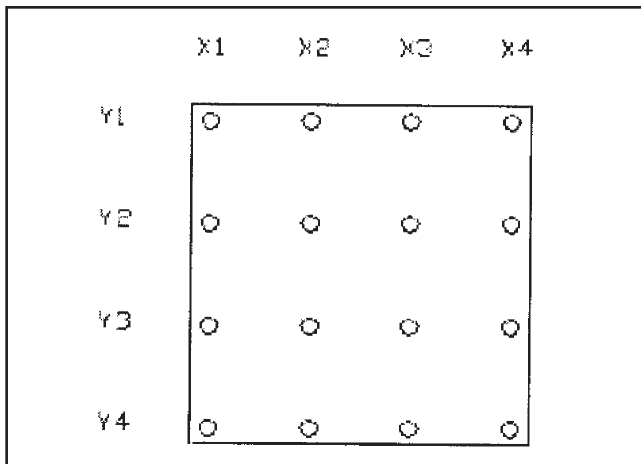


Fig. 10 — Example of 16 measuring points on the plate.

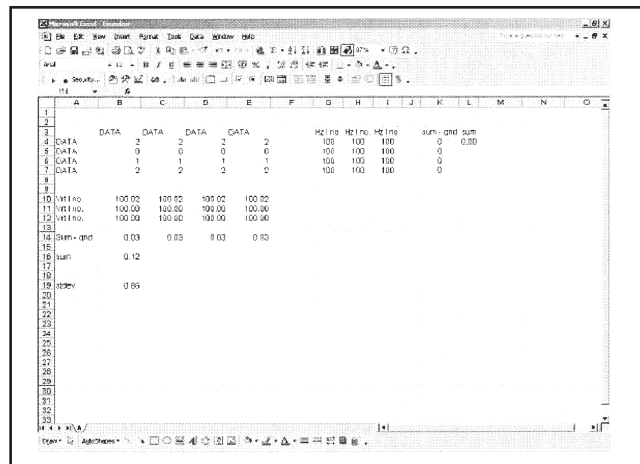


Fig. 11 — Excel spreadsheet showing the calculation process using the formulas provided.

Model Outputs

Predicted distortion at 72 points

Appendix 2

Two main flatness parameters have been used according to ASTM A568/A568-M 96 1996). The main use of I-numbers is found in steel sheet flatness applications (Ref. 29), where the two main characterizations in place, are steepness index and flatness index.

The steepness index is based on a representation of a sheet sample exhibiting edge waves of height H and an interval L, as shown in Fig. 1A.

The height H is typically in mm. The steepness index for the samples is defined by

$$S = H/L$$

However, it is normally expressed as a percentage:

$$\%S = (H/L) \times 100\%$$

If a series of lengthwise cuts is taken through the sheet shown in Fig. 1A, then the elastic stresses present are relaxed, and this results in narrow strips of differing lengths as shown in Fig. 2A.

Using the length of one of the strips as a reference (L_{ref}), the flatness index or the I-number value for an individual strip is defined as

$$I = (?L/L_{ref}) \times 10^5$$

where ?L = difference between the length of a given strip and the reference strip.

For the special case where waves or buckles are perfectly sinusoidal in character, the following relationship would apply between flatness and steepness:

$$I = [1/2 (H/L)]^2 \times 10^5 \quad \text{or} \\ I = 24.7S^2$$

The use of I-numbers and standard deviation together was found to describe the plate shape very accurately. It was also assumed that no two plates have the same I-

numbers and standard deviation, unless they are exactly the same shape.

Calculating I-Numbers

The calculation of I-numbers is based on the equations shown below.

$$I_y = \sum_{i=1}^{N_x} \sum_{j=2}^{N_y} \left(10000 + \frac{(H(i,j) - H(i,j-1))^2}{L^2} \right)^{1/2} - 100$$

$$I_x = \sum_{i=1}^{N_y} \sum_{j=2}^{N_x} \left(10000 + \frac{(H(j,i) - H(j-1,i))^2}{L^2} \right)^{1/2} - 100 \quad (A1)$$

This calculation must be carried out for each point on the plate. This can be easily done by setting out an Excel spreadsheet. The example in Fig. 3A has 16 measuring points. The I-number can be calculated for both the X and Y directions of the plate, which will describe the shape of the plate with two values. To do this, the distance between the measuring points has to be specified and kept constant. Using the marked grid system in the present work ensured that these criteria were met. If all of the points on the plate are the same value, then the plate is flat. In that case the I-number in the X direction would be 0 and in the Y direction it would also be zero.

If the plate has the shape shown below, then by examination the plate is distorted in the Y direction.

	X1	X2	X3	X4
Y1	2	2	2	2
Y2	0	0	0	0
Y3	1	1	1	1
Y4	2	2	2	2

The screen shot from the Microsoft Excel spreadsheet (Fig. 4A) shows how

the calculation process using Equation A1 can be greatly simplified.

The I-numbers would be as follows:

I in the X direction 0
I in the Y direction 0.12

For the next example, by examination the plate is distorted in the X direction.

	X1	X2	X3	X4
Y1	6	2	3	7
Y2	6	2	3	7
Y3	6	2	3	7
Y4	6	2	3	7

The I-numbers would be as follows

I in the X direction 0.66
I in the Y direction 0

For a plate distorted in the X and Y direction, as shown below,

	X1	X2	X3	X4
Y1	6	4	3	7
Y2	5	2	1	8
Y3	3	4	2	5
Y4	6	7	3	9

The I-numbers would be as follows:

I in the X direction 0.73
I in the Y direction 0.31

The larger the I-number, the greater the rate of change between each measurement, and so the greater will be the distortion in the plate.

Change of Address? Moving?

Make sure delivery of your *Welding Journal* is not interrupted. Contact the Membership Department with your new address information — (800) 443-9353, ext. 480; jleon@aws.org.

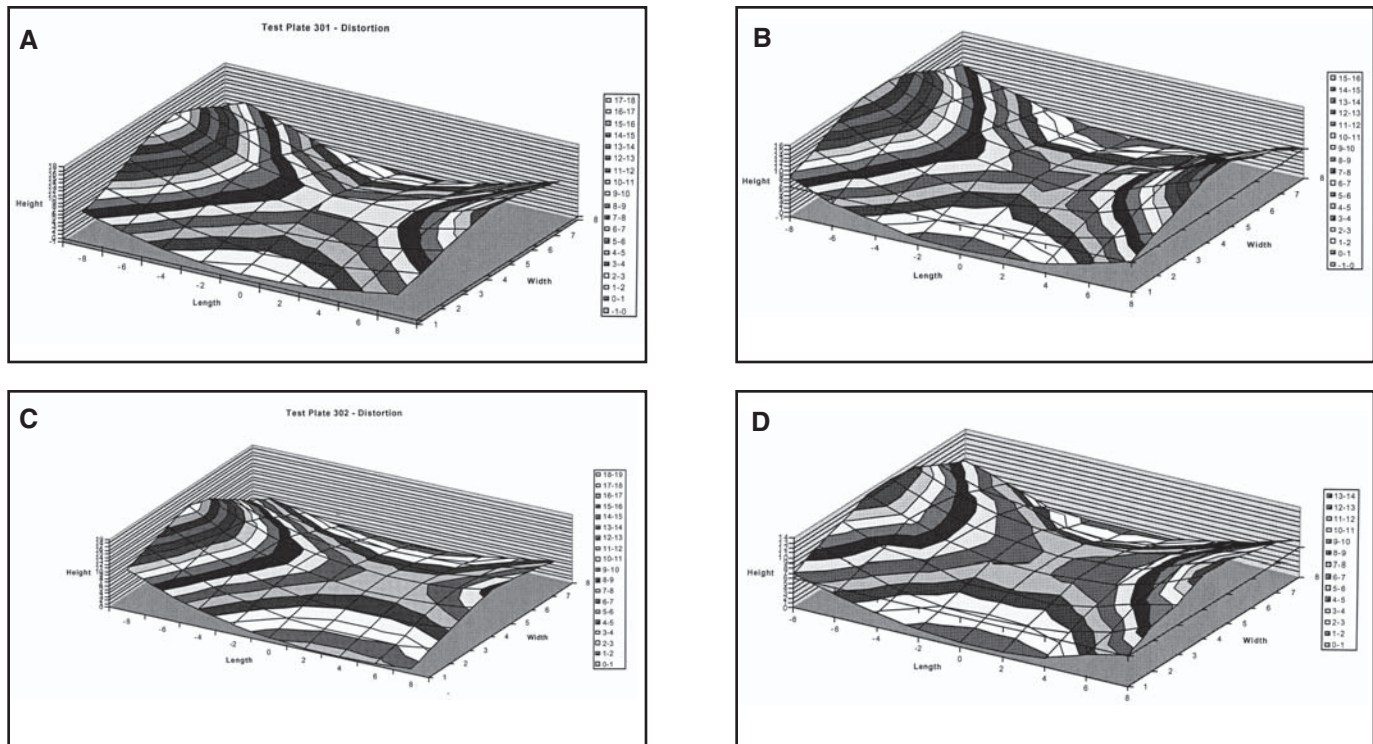


Fig. 4 — A — Actual distortion of a 6-mm plate of D grade steel (height in mm); B — distortion predicted from the model for the case shown in Fig. 4A. Overestimate between actual and predicted is 13% (height in mm); C — actual distortion of a 6-mm plate of D grade steel (height in mm); D — distortion predicted from the model for the case shown in Fig. 4C. Underestimate between actual and predicted is 18% (height in mm).

Table 3 — Trends from the Sensitivity Analysis Shown in Figure 5

Factor	Effect	Comments
Carbon equivalent	As CE increases the flatness improves	CE range -0.24-0.39
Carbon content	As carbon content increases, the flatness improves and then deteriorates after 0.125%C	C content range 0.09-0.15
Yield/tensile strength	As YS/TS increases, the flatness improves	YS/TS range 0.71-0.87
Plate treatment	Flatness deteriorated in the order As rolled-normalized rolled-normalized	
Heat input	As heat input increases, the flatness deteriorates	H.I. Range 0.145-0.195 kJ/mm ²

son was carried out on 6-mm-thick D-grade steel welded with the configuration shown in Fig. 2A.

When considering the 8-mm-thick plate, the exercise was repeated using 28 training data sets and 3 testing data sets. In this instance, the network architecture was a GFF with 16,000 iterations, 2 hidden layers, and a 0.7 momentum coefficient.

When the models were tested against four additional test plates (2 at 6 mm and 2 at 8 mm thick) it was found that good agreement was obtained with the 6-mm-thick material. However, there were significant discrepancies for the 8-mm-thick material. This appeared to be related to the complication of using two welding passes. It was decided to “lump” the two

welding passes into one, and reassess the model outputs. The practice of lumping weld passes has been used elsewhere (Ref. 21), and found to give acceptable results and also reduce processing time. In this specific case the data were assessed using the MLP model used for the 6-mm data.

At the start of the modeling, combining the 6- and 8-mm data was not considered, due to the effect of the second pass in the 8-mm-thick plate welding process. Based on the knowledge gained in this work, a different approach would be taken in the future that would lead to more versatility of the model.

The total inputs and ranges that were fed into the model are shown in Appendix 1, along with the outputs. This data set was

used to develop a software package called *PREDICTOR*, the details of which can be obtained elsewhere (Ref. 22).

Sensitivity of Outputs

The final developed model, containing both 6 mm and 8 mm lumped data, was run to determine which of the main inputs influenced the prediction of resultant weld distortion. The Sensitivity Analysis was carried out by the Neural Network Software called *NeuroSolutions*. Figure 5 shows the results of this. One factor that was found not to be sensitive was the initial tacked plate topology. Other work (Refs. 23, 24) has shown that the initial shape governs where subsequent weld-induced distortion is liable to occur. In summary, the most significant factors with sector of responsibility, in no specific priority, are as follows:

- Steel grade Steel mill
- Cutting process Shipyard
- Carbon equivalent (CE) Steel mill
but defined by Shipyard
- Yield/tensile strength ratio Steel mill
- Cutting process Shipyard
- Plate rolling treatment Steel mill

Each of these factors was examined in more detail, using standard deviation and I numbers as the indicator of distortion. The outcome of this is shown in Table 3.

A number of the factors shown are already well established in influencing dis-